Temperature-dependent single-particle properties of the two-dimensional Hubbard model

V. Zlatić
Institute of Physics, Zagreb, Croatia

S. Grabowski and P. Entel
Duisburg University, D-47 048 Duisburg, Germany
(Received 24 February 1997)

The temperature-dependent self-energy of the hole-doped two-dimensional Hubbard model is calculated perturbatively up to second order and used to find the spectral function for all points in the Brillouin zone. Single-particle dispersion, density of states, and Fermi surface topology are thus obtained and the appearance of the strong-coupling features studied. The renormalized quantities are temperature dependent due to an interplay between the electron correlation and topology of free-electron bands close to the Fermi energy. [S0163-1829(97)01548-8]

Single-particle excitations of the hole-doped two-dimensional (2D) Hubbard model often have been discussed recently in connection with the electronic properties of metallic cuprates.[1–6] For small correlation U, or large doping, the model is in the weak-coupling regime, where the spectral function $A_{\mathbf{p}}(\omega)$ has the usual Fermi liquid form, the single-particle excitations are well described by uncorrelated dispersion, $\omega^0_{\mathbf{p}}=\epsilon_{\mathbf{p}}-\mu$, and the uncorrelated band-width $W=8t_x$ provides the only characteristic energy scale. Here $\epsilon_{\mathbf{p}}=-2t_x\cos(p_xa_x)-2t_y\cos(p_ya_y)$, $\mathbf{p}$ denotes a point in the Brillouin zone (BZ), μ is the chemical potential, and t_x, t_y are the nearest neighbor hoppings in the x and y directions, respectively. For large enough U and small doping, different strong-coupling features appear. In that regime, at low temperatures, the position of the low-energy peak of $A_{\mathbf{p}}(\omega)$ still defines the quasiparticle (QP) excitations $\omega_{\mathbf{p}}$, but dispersion is reduced with respect to $\omega^0_{\mathbf{p}}$. The width of the QP band between $(\pi,0)$ and (π,π) defines the low-energy scale $J(U)$ such that the system behaves differently for $T\ll J$ and $T\gg J$.

Experimentally, the single-particle excitations are probed by angular resolved photoemission;[7,8] these measurements provide information on $A_{\mathbf{p}}(\omega)$ and $\omega_{\mathbf{p}}$ as a function of angle (momentum) and energy. The room-temperature data on cuprate superconductors reveal an open Fermi surface, indicate the presence of flat bands close to $(\pi,0)$ and $(0,\pi)$, and show an anomalously low-energy scale in the proximity of the Fermi energy E_F. To compare the spectroscopic data with theoretical predictions, one has to calculate the single-particle excitations as a function of temperatures and doping.

Insight into the spectral properties of the 2D Hubbard model for $T\geqslant J$ has been obtained recently by quantum Monte Carlo (QMC) calculations[9,10] and by exact diagonalization.[11] Thus it is found that at small doping strongly correlated features set in for $U\geqslant W/2$. However, the low-T shape of the Fermi surface and the details of the dispersion in the metallic region are difficult to obtain in such a way because QMC and exact diagonalizations are limited to rather small clusters and high temperatures. Here we use perturbation theory and evaluate the spectral properties of hole-doped model in the full temperature range and up to intermediate values of U. We notice that the weak-coupling regime breaks down for relatively small U and find the strong-coupling features for $U\geqslant W/2$. The perturbation calculations are straightforward to do and, on a standard UNIX station, the spectral function is obtained in a few minutes for all the points in the BZ, even for systems with $N=256\times256$ lattice sites.[12]

Renormalized spectral properties are obtained from the Dyson equation, which gives

$$A_{\mathbf{p}}(\omega,T)=-\frac{1}{\pi}\mathrm{Im}\frac{1}{\omega+i\eta-(\epsilon_{\mathbf{p}}-\mu)-\Sigma^{(2)}_{\mathbf{p}}(\omega,T)}, \quad (1)$$

where $\Sigma^{(2)}_{\mathbf{p}}(\omega,T)$ is the single-particle self-energy and ω is measured with respect to μ in units of t_x. From $A_{\mathbf{p}}(\omega)$ we obtain the renormalized dispersion, the temperature dependence of the Fermi surface, and the density of states $\rho(\omega,T)=(1/N)\Sigma_{\mathbf{p}}A_{\mathbf{p}}(\omega,T)$. The renormalized particle number is $n_e(\mu)=2\int d\omega\rho(\omega)f(\omega)$, where $f(\omega)$ is the Fermi function. Temperature is controlled by dimensionless parameter βt_x ($\beta=1/k_BT$) and μ is adjusted so as to keep $n_e(T)=0.8$ for each value of U and β.

The calculations are performed by writting the Hubbard Hamiltonian as $H=H_{MF}+H'_U$, where H_{MF} describes the mean-field state and H'_U defines the repulsive interaction between two particles of opposite spin at the same site (with the mean-field value subtracted),

$$H'_U=U\sum_{i=1}^{N}(n_{i\uparrow}-\langle n_{i\uparrow}\rangle)(n_{i\downarrow}-\langle n_{i\downarrow}\rangle). \quad (2)$$

The self-energy is then generated by the perturbation expansion with U as the expansion parameter. It is easy to show (for detailes see Ref. 4) that $\Sigma^{(2)}_{\mathbf{p}}(\omega,T)$ is given by the Fourier transform of the space-time self-energy $\Sigma^{(2)}_{\mathbf{R}}(t)=[a^2_{\mathbf{R}}(t)b_{-\mathbf{R}}(-t)+a_{-\mathbf{R}}(-t)b^2_{\mathbf{R}}(t)]$, where $a_{\mathbf{R}}(t)=(1/N)\Sigma_{\mathbf{p}}\exp i(\mathbf{pR}-\epsilon_{\mathbf{p}}t)f(\epsilon_{\mathbf{p}}-\mu)$ and $b_{\mathbf{R}}(t)=(1/N)\Sigma_{\mathbf{p}}\exp i(\mathbf{pR}-\epsilon_{\mathbf{p}}t)[1-f(\epsilon_{\mathbf{p}}-\mu)]$. The $\mathbf{p}$ summations run

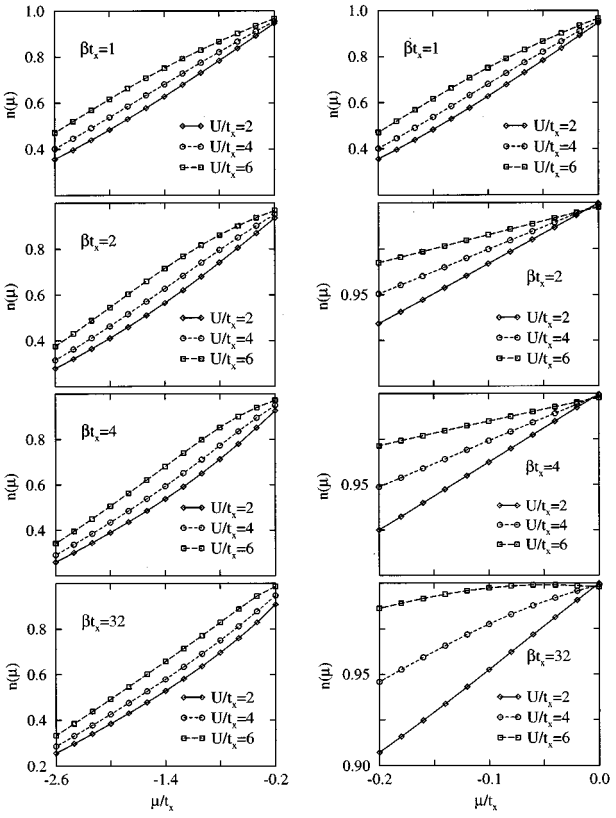

FIG. 1. Particle number $n(\mu)$ plotted versus μ for $U/t_x=2$, 4, and 6 at temperatures $\beta t_x=1$, 2, 4, and 32.

over the full BZ and for periodic systems can be performed exactly by a fast Fourier transform algorithm.

The properties of $\Sigma_{\mathbf{p}}^{(2)}(\omega,T)$ are described in Ref. 13 and we recall only that the effects of temperature are most pronounced at low energies, where the slope of $\mathrm{Re}\Sigma_{\mathbf{p}}^{(2)}(\omega,T)$ changes sign and the magnitude of $\mathrm{Im}\Sigma_{\mathbf{p}}^{(2)}(\omega,T)$ increases linearly with T. For $T>J$, damping exceeds the energy of excitations and the quasiparticles cease to be well defined. The anisotropy of $\Sigma_{\mathbf{p}}^{(2)}(\omega,T)$ in the BZ, which marks the $T=0$ result,[4] is reduced by the increase of temperature. We notice that for $U\geqslant W/2$ and $n_e=0.8$ the self-energy gives rise to qualitatively different spectral features, but emphasize that the description of the strong coupling regime by second-order approximation requires some care.

The problems encountered by straightforward perturbation theory for large values of U are illustrated in Fig. 1, where $n_e(\mu)$ is plotted for $\beta t_x=32$, 4, 2, and 1 and $U/t_x=6$, 3, and 2. These curves, which are parametrized by U and T, provide μ, which corresponds to $n_e=0.8$. Figure 1 shows that the correlation shift $n_e(\mu)$ curves upward and reduces the slope of $n_e(\mu)$ in the small-μ ($n_e\simeq 1$) region, which is in agreement with QMC simulations for doped systems.[14] Close to $\mu=0$, where $n_e=1$, the low-T charge susceptibility $\chi_c\simeq\partial n_e/\partial\mu$ becomes very small,[14] as expected for systems driven by correlations towards an insulating state with a gap in the excitation spectrum. (Note that $\chi_c=0$ for μ within the gap.) However, for sufficiently large correlations $\Sigma_{\mathbf{p}}^{(2)}(\omega,T)$ leads to $n_e(\mu)$ with a negative slope around $\mu=0$, which is unphysical. Thus the renormalization of $G_{\mathbf{p}}(\omega,T)$ by

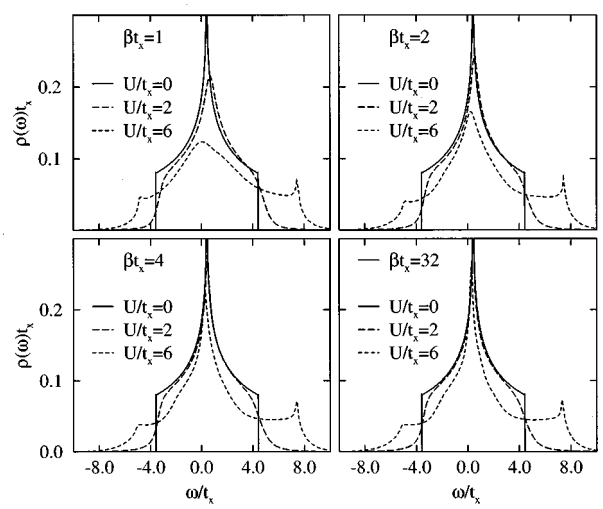

FIG. 2. Density of states $\rho(\omega)$ plotted versus ω for $n_e=0.8$ and $U/t_x=0$, 2, and 6 at temperatures $\beta t_x=1$, 2, 4, and 32.

$\Sigma_{\mathbf{p}}^{(2)}(\omega,T)$ has to be supplemented by the condition $\partial n_e/\partial\mu\geqslant 0$, which limits the value of U in the Dyson equation. For $n_e=0.8$ and $U/t_x\simeq 6$ the system is already in the strongly correlated regime and we still have $\chi_c>0$. The anomalous shape of $\partial n_e/\partial\mu$ deduced from Fig. 1 is due to an interplay between the on-site correlation and the Van Hove singularities that apear in $\omega_{\mathbf{p}}^0$. Temperature has a very strong effect on $n_e(\mu)$ for small μ; one finds that $\partial n_e/\partial\mu$ changes substantially between $\beta t_x=4$ (the lowest temperature used in QMC simulations) and $\beta t_x=32$. For $Ut_x\leqslant 6$, the reduction of temperature below $\beta t_x=32$ does not lead to any further renormalization of the low-energy properties. Note that χ_c calculated from Eq. (1) and $\Sigma_{\mathbf{p}}^{(2)}(\omega,T)$ is very close to the results of Ref. 15, obtained by expanding the two-particle correlation functions up to U^2.

The temperature dependence of $\rho(\omega)$ calculated for $U/t_x=6$, 2, and 0 is shown in Fig. 2 for $\beta t_x=32$, 4, 2, and 1. The Van Hove singularity in the uncorrelated density of states is located above E_F since $n_e=0.8$. At low temperatures, $\rho(\omega)$ shows for large U a characteristic triple-peaked structure: a narrow singularity around E_F and broad wings at very high energies. The correlations shift the singularity towards E_F and reduce its spectral intensity. The low-energy peak persists up to $\beta t_x=4$, but the transfer of spectral weight out of the low energy region is found at all temperatures. The high-T shape of $\rho(\omega)$ relates mainly to the temperature dependence of $\mathrm{Im}\Sigma_{\mathbf{p}}(\omega,T)$.

Properties of $A_{\mathbf{p}}(\omega,T)$ for $U/t_x=6$ and $\beta t_x=32$, 4, 2, and 1 are shown in Fig. 3 along several cuts through the BZ. The low-energy peak defines $\omega_{\mathbf{p}}(T)$, while the high-energy peaks correspond to Hubbard excitations.[4] These two types of excitations are found at all temperatures and for all points in the BZ, although the shape and the relative weight of the Hubbard and QP excitations change with temperature. For $\omega_{\mathbf{p}}/W\ll 1$ the position of the QP peak (indicated by dots in Fig. 3 coincides with the solution of secular equation $\omega_{\mathbf{p}}^*(T)=(\epsilon_{\mathbf{p}}-\mu)+\mathrm{Re}\Sigma_{\mathbf{p}}(\omega_{\mathbf{p}}^*)$. At $T=0$, we find on the Fermi surface $A_{\mathbf{p}_F}(\omega)\simeq Z_{\mathbf{p}_F}\delta(\omega-\omega_{\mathbf{p}_F}^*)$, where $Z_{\mathbf{p}_F}$ describes the reduction of the quasiparticle weight due to self-energy

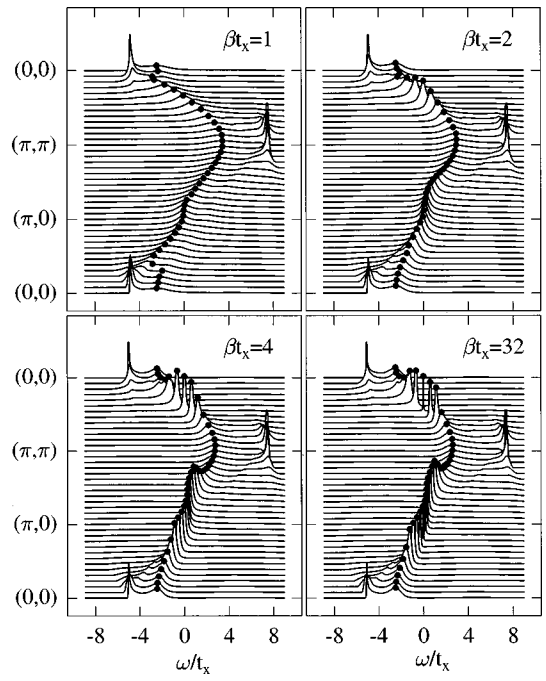

FIG. 3. Single-particle spectral function $A^{\mu}_{\mathbf{p}}(\omega)$ plotted versus ω along high-symmetry cuts through the Brillouin zone for $n_e=0.8$ and $U/t_x=6$ at temperatures $\beta t_x=1$, 2, 4, and 32. The dots mark the positions of the quasiparticle peaks.

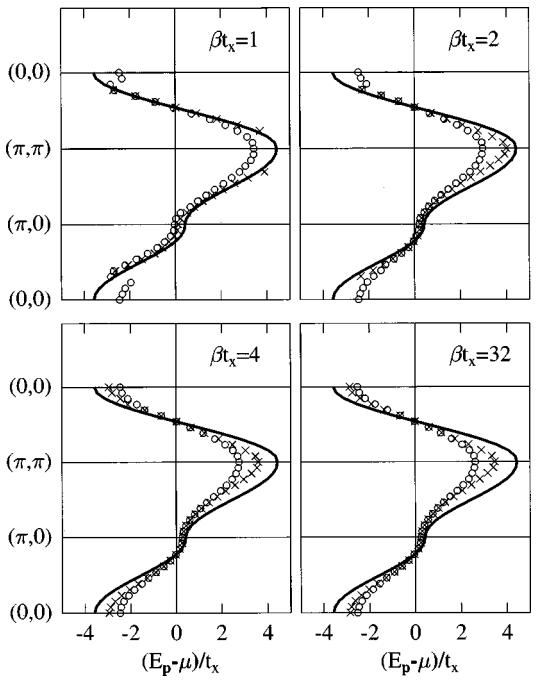

FIG. 4. Renormalized dispersion plotted versus $\mathbf{p}$ for $n_e=0.8$ and $U/t_x=6$ at temperatures $\beta t_x=1$, 2, 4, and 32. Open symbols indicate the peak positions of the spectral function, crosses show the dispersion obtained from the secular equation, and the full lines display the dispersion of the noninteracting system.

corrections $1/Z_{\mathbf{p}_F}=1-\partial \mathrm{Re}\Sigma_{\mathbf{p}}(\omega)/\partial\omega|_{\omega^*_{\mathbf{p}_F}}$. Close to half filling we find that $Z_{\mathbf{p}_F}$ is rapidly reduced by U. In the proximity of the Fermi surface, the renormalized QP are well defined, but since $\mathrm{Im}\Sigma_{\mathbf{p}}(0)=0$, $A_{\mathbf{p}}(\omega)$ is split into two asymmetric peaks located at the opposite sides of E_F. At elevated temperatures the QP peak broadens and for $T\geqslant J$ merges with the background; here the propagation is completely incoherent due to large damping. Far away from the Fermi surface the QP peak is always rather broad. The sharpness of the Hubbard peak found for $\mathbf{p}$ in the vicinity of $(0,0)$ and (π,π) is an artifact of the second order approximation. This high-energy peak becomes singular for $T=0$ because the secular equation has a solution at $|\omega^*_{\mathbf{p}}|>W/2$, where $\mathrm{Im}\Sigma^{(2)}_{\mathbf{p}}(\omega^*_{\mathbf{p}})=0$. However, the phase-space restrictions that make $\mathrm{Im}\Sigma^{(2)}_{\mathbf{p}}(\omega)$ band limited are removed by higher-order diagrams, which makes the high-energy spectral weight incoherent.

Renormalized QP dispersion defined by the momentum dependence of $\omega_{\mathbf{p}}(T)$ is shown in Fig. 4. Circles show the dispersion corresponding to Fig. 3, crosses represent $\omega^*_{\mathbf{p}}$, while the full line gives $\omega^0_{\mathbf{p}}$. At low temperatures, the reduction of the width of the QP band is particularly pronounced between the $(\pi,0)$ and $(\pi/2,\pi/2)$ points in the BZ. Thus correlations generate a low-energy scale J and expand the saddle points in the BZ. At $T=0$ we find $J/t_x=2$ for $U/t_x=6$. The increase of temperature shifts the saddle points to lower energies and broadens the overall QP bandwidth.

The temperature dependence of the renormalized Fermi surface is shown in Figs. 5(a) and Fig. 5(b) for $\beta t=32$, 4, 1 and two values of U. Figure 5(a) is obtained by using the condition $n_{\mathbf{p}_F}=\int d\omega f(\omega)A_{\mathbf{p}_F}(\omega,T)=1/2$, while Fig. 5(b) is obtained by using $\omega_{\mathbf{p}_F}=0$. At low T, where both definitions lead to identical results, the Fermi surface centers at $(0,0)$ and encloses the volume v_F, which is very nearly equal to $n_e(U,T)$. For $U/t_x=6$ we find a small deviation from the Luttinger theorem, $(v_F-n_e)/n_e\simeq 0.01$, which is due to the fact that $n_e(U,T)$ is calculated by substituting $\Sigma^{(2)}_{\mathbf{p}}(\omega)$ into the Dyson equation.[16] For small U the Fermi surface expands with T, regardless of definition. For large U the Fermi surface in Fig. 5(a) shrinks and that in Fig. 5(b) expands with T. For large enough T, the Fermi surface in Fig. 5(b) becomes nested and then closes around (π,π).

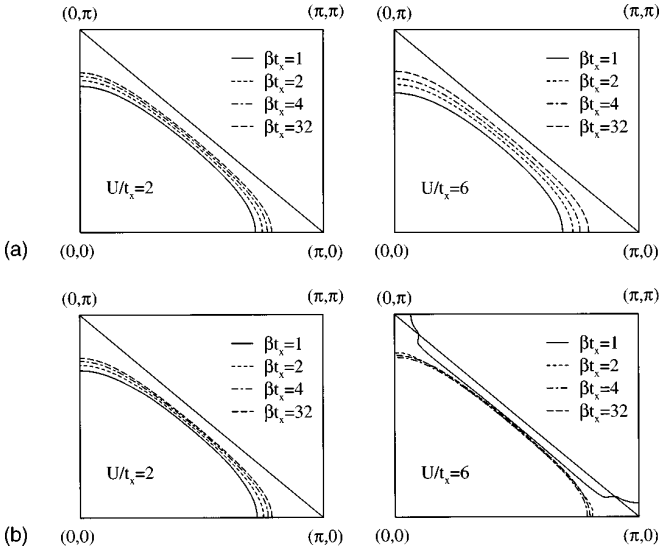

FIG. 5. Renormalized Fermi surface corresponding to $n_e=0.8$ shown for $U/t_x=2$ and 6 at temperatures $\beta t_x=1$, 2, 4, and 32. In (a) $\mathbf{p}_F$ is defined by $n_{\mathbf{p}_F}=1/2$, while in (b) we use $\omega_{\mathbf{p}_F}=0$.

Finally, we remark that the imaginary-time Green's function calculated by second-order perturbation theory agrees surprisingly well with the QMC data.[17,18] On the real axis, our high-T results for $A_{\mathbf{p}}(\omega,T)$ are qualitatively similar to the QMC results.[9,10] Both methods lead to incoherent excitations at high energies and QP excitations at low energies and show that close to the Fermi surface the coherent spectral weight is rapidly suppressed by U. The QP dispersion obtained by perturbation expansion agrees with QMC calculations[9,10] in large parts of the BZ, but poor agreement is found around the antiferromagnetic (π,π) point. Thus, for large values of U, the low-energy scale provided by $\Sigma_{\mathbf{p}}^{(2)}(\omega)$ does not reproduce quantitatively the QMC scale. Since for very large U the present approximation leads to incorrect χ_c, it is not surprising that for $U/t_x=6$ only a qualitative agreement with the QMC data[9,10] is found. Here we notice that the full spectral function obtained by perturbation expansion and QMC is very different from the one obtained by the fluctuating exchange approximation[5] (FLEX): the triple-peaked structure that is found in $A_{\mathbf{p}}(\omega,T)$ and $\rho(\omega,T)$ by perturbation expansion and QMC is not present in the FLEX data. Thus, nearly perfect agreement between FLEX (Ref. 5) and QMC (Refs. 9 and 10) calculations regarding the QP dispersion is somewhat surprising.

In summary, we studied the spectral properties of the 2D Hubbard model with 0.8 electrons, using the perturbation expansion above the paramagnetic metallic state. For large U and small doping, we find reduced QP dispersion and a dynamically generated, low-energy scale J. In this regime, the position and the relative weight of QP and Hubbard excitations are found to be strongly temperature dependent. The spectral function and the density of states have at low temperatures a characteristic triple-peaked structure. Correlations reduce the singular spectral weight and shift it towards E_F. The doping and temperature dependence of n_e indicate that correlations suppress χ_c and drive the system closer to a metal-insulator transition. The topology of the Fermi surface determined from the QP dispersion is also found to be temperature dependent. Our results show many features seen in the spectroscopic data,[7,8] which might be taken as an indication that the large-U limit of the 2D Hubbard model describes the essential properties of metallic cuprates.

Financial support from the Alexander von Humboldt Foundation and the Sonderforschungsbereich 166 Duisburg/Bochum is gratefully acknowledged.

[1] P. W. Anderson, Science **256**, 1526 (1992).
[2] H. Schweitzer and G. Czycholl, Z. Phys. B **83**, 93 (1991).
[3] J. Galán *et al.*, Phys. Rev. B **48**, 13 654 (1993).
[4] V. Zlatić *et al.*, Phys. Rev. B **52**, 3639 (1995).
[5] M. Langer *et al.*, Phys. Rev. Lett. **75**, 4508 (1995).
[6] V. Zlatić *et al.*, Europhys. Lett. **34**, 693 (1996);
[7] Z. -X. Shen and D. S. Dessau, Phys. Rep. **253**, 1 (1995).
[8] P. Aebi *et al.*, Phys. Rev. Lett. **72**, 2757 (1994).
[9] N. Bulut *et al.*, Phys. Rev. B **50**, 7215 (1994); Phys. Rev. Lett. **72**, 705 (1994).
[10] R. Preuss *et al.*, Phys. Rev. Lett. **75**, 1344 (1995).
[11] E. Dagotto, Rev. Mod. Phys. **66**, 763 (1994).
[12] The self-contained FORTRAN programs that give $\Sigma_{\mathbf{p}}^{(2)}(\omega)$ and $A_{\mathbf{p}}^{(2)}(\omega)$ are available from the authors upon request (electronic address: zlatic@ifs.hr).
[13] V. Zlatić, Physica B **230-232**, 75 (1997).
[14] A. Moreo and D. Duffy, J. Low Temp. Phys. **99**, 311 (1995).
[15] T. Hotta and S. Fujimoto, Phys. Rev. B **54**, 5381 (1996).
[16] C. J. Halboth and W. Metzner, Z. Phys. B **102**, 501 (1997).
[17] N. E. Bickers and S. W. White, Phys. Rev. B **43**, 8044 (1994).
[18] Y. M. Vilk and A.-M. S. Tremblay, Europhys. Lett. **33**, 159 (1996); .